Harmonic cross phase modulation in ZnSe

P. P. Ho, Q. Z. Wang, D. Ji, T. Jimbo, and R. R. Alfano
Institute for Ultrafast Spectroscopy and Lasers, Photonic Application Laboratory, Departments of Electrical Engineering and Physics, The City College of New York, New York, New York 10031

(Received 25 April 1988; accepted for publication 26 October 1988)

The temporal profiles of harmonic cross phase modulation pulses from 500 to 570 nm generated in ZnSe by a 1054 nm picosecond pulse have been observed and theoretically modeled. The pulse shape of these harmonic-modulated pulses is accounted for by the interference and induced phase matching of the harmonic generated waves in ZnSe by cross phase modulation.

When two laser pulses of different frequencies propagate simultaneously in matter, coupled interactions occur through the third-order susceptibility.[1–8] This leads to the cross phase modulation[1–6] where the spectral bandwidth of both pulses increases. The generation process provides knowledge about multiwave interactions with matter and quantum nondemolition detection[7] applications in lasers and communications. In this letter we report on a new class of cross phase modulation (XPM) process resulting from the coupling of the second-order and the third-order susceptibilities in ZnSe. The temporal property of the induced spectral broadened pulses of a weak second-harmonic signal has been measured and theoretically fitted.

The experimental setup is shown in Fig. 1. An 8 ps, 2 mJ, 1054 nm laser pulse was weakly focused into the ZnSe sample. The spot size at the sample was about 1.5 mm in diameter. The second-harmonic produced in ZnSe samples was about 10 nJ. The incident laser energy was controlled by changing the neutral density filter. The output signal was sent through a 1/2 Jarrell–Ash spectrograph to measure the spectral distribution of the signal light. A reference pulse at 527 nm was produced in a potassium dihydrophosphate crystal. Using a beamsplitter, 1054 and 527 nm pulses were separated into two different paths. The weak 527 nm reference pulse was used for calibration and passed through a fixed distance in air to set the zero reference time for the streak camera. Only a 1054 nm pulse was used to pump the ZnSe samples. The pump pulse was almost collimated through the entire length of the sample. The temporal profile and the propagation time of the pulses which exited from the ZnSe and the reference 527 nm pulse were measured by a Hamamatsu 2 ps resolution streak camera system.[9] The zero time between reference 527 nm and sample pump 1054 nm was determined. The absolute time delay for the spectral broadened pulse traveling through the sample was determined by measuring the time separation between the 527 nm reference pulse beam and the spectral broadened signals in the streak camera. Polycrystalline ZnSe samples of thickness 2, 5, 10, 22, and 50 mm were purchased from Janos Inc. and a single-crystal ZnSe of 16 mm thickness was grown at Philips.[1]

Measurements of ZnSe SHG XPM spectra[1] indicated that the extent of the spectral broadening about the second-harmonic line at 527 nm depended on the intensity of the incident 1054 nm laser pulse. When the incident laser pulse energy was 2 mJ, there was significant spectral broadening from 500 to 570 nm. There was no significant difference in the spectral broadening distribution measured in the single and polycrystalline materials. A typical spectrum of the SHG XPM is displayed in Fig. 2. When the incident pulse energy was less than 1 mJ, the spectral broadening was found to depend monotonically on the pulse energy of 1054 nm.

The temporal profile and propagation time of an intense 1054 nm pump pulse and induced spectral broadened pulses propagating through a 22 mm ZnSe polycrystalline sample are shown in Fig. 3. A pulse delay of ~ 189 ps at 1054 nm was observed in Fig. 3(a) when an intense 1054 nm pulse passed through the crystal, while the total signal of SHG and SHG XPM with wavelength spread from 500 to 570 nm displayed in Fig. 3(b) indicated a sharp spike at 189 ps and a long plateau spanned from 189 to 249 ps. Using 10 nm bandwidth narrowband filters, pulses of selected wavelengths from the SHG XPM have also been measured. For example, in Figs. 3(c) and 3(d), the temporal distribution of two pulses with wavelengths centered at 530 nm and 550 nm is displayed, respectively. All traces from Figs. 3(b)–3(d) indicated that the induced spectral broadened pulses have one major component emitted at nearly the same time as the 1054 nm incident pulse [Fig. 3(a)]. The selected 10 nm SHG XPM away from the SH wavelength has shown a dominant pulse distribution generated at the the end of the crystal. Furthermore, when a weak 3 nJ, 527 nm calibration pulse propagated alone through the 22 mm ZnSe, a propagation time of about 249 ps was observed as the expected group velocity. The measured as well as the calculated values[10] of

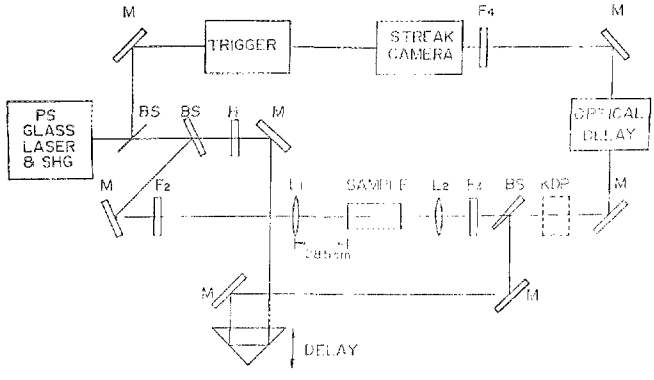

FIG. 1. Experimental setup to measure the temporal profile and propagation time of the pulses. BS: beamsplitter; F_i: color and neutral density filter set; M: mirrors; L_i: lens; F_3: color and narrowband filters to select particular signal wavelength; F_4: set of neutral density filters to control the light intensity before entering streak camera; dashed KDP: 100-μm-thick KDP crystal which was only inserted during the measurement of the propagation delay time of the 1054 nm pump pulse traveled through air or ZnSe.

 0003-6951/89/020111-03$01.00

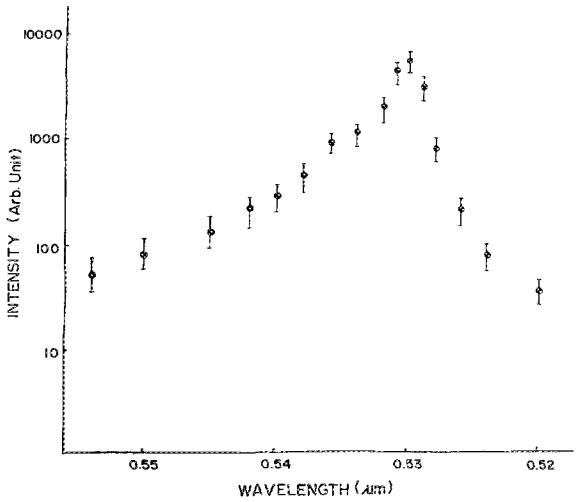

FIG. 2. Spectral measurement of the induced spectral broadened pulse around the SH by sending a 1054 nm pulse through a 22 mm ZnSe.

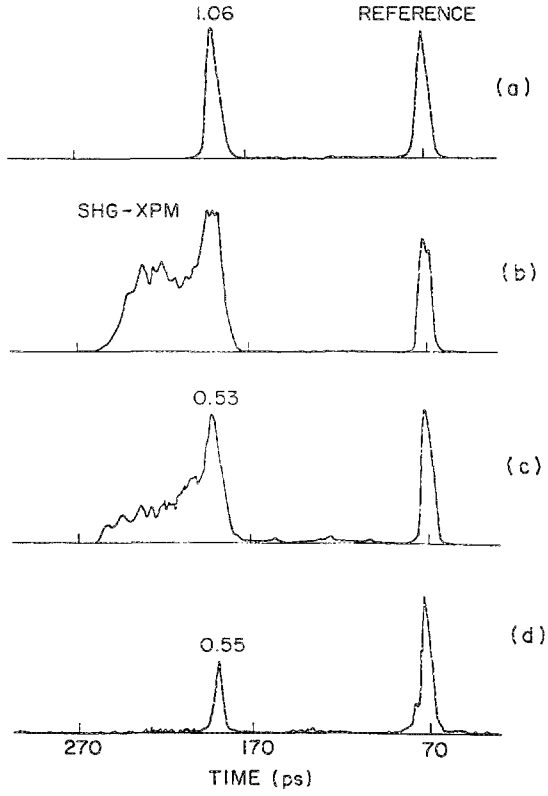

FIG. 3. Temporal profile and propagation delay time of (a) incident 1054 nm, (b) SHG XPM signal of all visible spectra, (c) selected 530 nm from SHG XPM, and (d) selected 550 nm from SHG XPM of a 22-mm-long ZnSe crystal measured by a 2 ps resolution streak camera system. The reference time corresponds to a laser pulse traveling through air without the crystal. The right-hand side of the time scale is the leading time. The vertical scale is an arbitrary intensity scale.

the group refractive indice of ZnSe are $n_{g,527} = 3.39$ and $n_{g,1054} = 2.57$.

A second-harmonic cross phase modulation model is used to explain our observations of temporal and spectral behavior of the induced spectral broadening in ZnSe. This analysis is similar to the theoretical analysis of Raman XPM process.[6] When an intense laser pulse propagates through noncentrosymmetric media where both χ^2 and χ^3 are operative, coupled spectral broadening around the second-harmonic frequency occurs. The first-order partial differential equations[11,12] for the pulses can be written as

$$\frac{\partial E_{10}}{\partial z} + \frac{1}{v_1}\frac{\partial E_{10}}{\partial t} = i\gamma |E_{10}|^2 E_{10}, \tag{1}$$

$$\frac{\partial E_{20}}{\partial z} + \frac{1}{v_2}\frac{\partial E_{20}}{\partial z} = \underbrace{\frac{i\sigma E_{10}^2 \exp[-i(k_2 - 2k_1)z]}{\text{SHG}}}_{\text{SHG}} + \underbrace{\frac{2i\gamma |E_{10}|^2 E_{20}}{\text{XPM}}}_{\text{XPM}} - \underbrace{\frac{\alpha E_{20}}{\text{Absorption}}}_{\text{Absorption}}, \tag{2}$$

in the slowly varying time and space envelope approximation. High-order derivatives of the wave equation are neglected. The E_{20} signal is weak in comparison to the pump pulse. Functions E_{10} and E_{20} are the electric field envelope amplitudes, v_1 and v_2 are group velocities, k_1 and k_2 are wave vectors for ω and 2ω pulses, respectively. Parameter α is the absorption coefficient at 2ω, $\sigma = \mu_0 \omega c \chi^2/2$, χ^2 is the second-order nonlinearity, $\gamma = 3\omega^2 \mu_0 \chi^3/8k_1$, and χ^3 is the third-order nonlinearity.

The solution for E_{20} from the coupled equations can be written as[2]

$$E_{20} = i\sigma A_0 \exp\left[-\alpha z + i(2\gamma A_0^2)\int_0^z F^2(U+\eta z')dz'\right] \times \int_0^z F^2(U+\eta z')\exp(\alpha z') \times \exp\left[-i\xi z' + i2\gamma A_0^2 F^2(U+\eta z')z' - 2i\gamma A_0^2 \int_0^{z'} F^2(U+\eta z'')dz''\right]dz' \tag{3}$$

where $U = (t - z/v_2)/\tau$, $\eta = (n_2 - n_1)/c\tau$, $\xi = (n_2^p - n_1^p)2\omega/c$, n_1, n_1^p, n_2, and n_2^p are the group and phase indices of refraction at ω and 2ω, respectively, A_0 is the initial amplitude of ω pulse, F is the pulse envelope function, and τ is the pulse duration parameter.

A theoretical curve is plotted in Fig. 4 using Eq. (3) and appropriate constant parameters used in the experiment. The calculated temporal distribution of SHG XPM is strongly affected by the nonphase-matched coefficient: $\Delta kz' = -\xi z' + i2\gamma A_0^2 F^2(U+\eta z')z' - 2i\gamma A_0^2 \int_0^{z'} F^2(U + \eta z'')dz''$. The first term of $\xi z'$ for $\Delta kz'$ is a conventional (self) nonphase-matched term due to the crystal dispersion property. The second and third terms of $\Delta kz'$ which depend on the third-order susceptibility γ and incident laser power A^2 can be called the *induced* nonphase-matched term which helps in canceling out the first term of mismatch.

In a conventional SHG where $\gamma A^2 = 0$, the self-nonphase-matched term will determine the pulse shape of the SHG waves. The SHG signal will only be observed within the given coherence lengh $(1/\Delta k)$ of the nonlinear crystal and washed out at all other places. As long as the index difference and the crystal length are large enough, two separated peaks in time may be observed under the assumption of a nondepleted input and no absorption of the generated pulse. The peak separation is $\sim \Delta nL/c$.

When $\gamma A^2 \neq 0$, the Δk term will be influenced by both the self and induced nonphase-matched terms. Since the in-

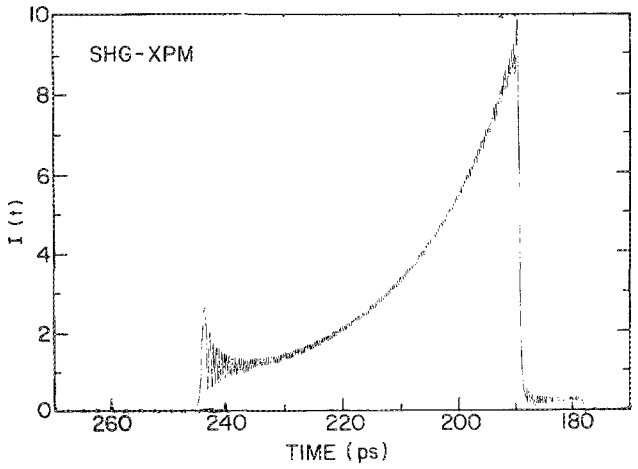

FIG. 4. Theoretical calculated curve of the temporal distribution of SHG XPM from Eq. (3). The following parameters have been chosen: $z = 22$ mm, $\tau = 6.79$ ps, $\alpha = 0.3 + 0.23 \times 10^{-4}(\gamma A^2)$ cm^{-1}, where 0.3 is the linear absorption coefficient and the second term is the induced absorption coefficient, $n_2 - n_1 = 0.78$, $n_2^0 - n_1^0 = 2.697 - 2.484 \sim 0.21$, and $\gamma A_0^2 = 10^4$ cm^{-1}.

duced-nonphase-matched term depends on the time varying pulse envelope function F^2, Δk will vary as a function of time and space and modulated by the terms of γ and A^2. This modulated noncancellation pulse shape can be clearly observed in both the experimental curve of Fig. 3(b) and calculated curve Fig. 4. Induced-nonphase-matched terms destroy the interference pattern of the SHG waves which oscillates at a nonuniform period canceling the generation of SH inside the crystal. Furthermore, in a numerical computer calculation with a fixed ξ, the magnitude of the noncancellation middle portion of the XPM pulse reduces as γA_0^2 decreases.

In addition, as shown in Fig. 3(b), the total SHG XPM wave emitted at the exit surface was more than that from the entrance surface of ZnSe. This can be accounted by the absorption in ZnSe (includes linear absorption and two-photon induced absorption[13] via the imaginary part[14] of χ^3). The peak generated from the front entrance of the crystal is reduced. Newly generated SHG XPM wavelengths appear mainly to be emitted at the exit surface of the crystal.

There are several other possible mechanisms for the observed temporal behavior of the SHG and its spectral broadened pulses. The first possible model is the enhanced surface phenomenon such as the SHG of the self-phase modulation (SPM) process of 1054 nm. However, three observations contradict the surface model. First, the signal of the induced spectral broadened pulse was found to vary linearly with the sample thickness from 2 to 22 mm. Second, there was no difference in the output intensity or time dynamics of induce broadened spectra when the ZnSe as placed in ethylene glycol or CS_2 to reduce the index mismatch between the crystal and air. Third, using different ZnSe crystals with varied surface roughness, the output spectral broadened signal intensity remained to be the same. These three observations rule out the possibility of surface effect. The second possibility is the compensation of the group velocity dispersion in ZnSe by the negative nonlinear index of refraction.[15] However, no apparent change was observed in our measurements. The third possible model is the two-photon-like excitonic polariton.[16] This model is also ruled out from a temperature-independent measurement of the output signal strength. The output spectral broadened pulse intensity remained the same from 4 to 300 K.

The sharp spike of the selected 550 nm pulse profile in Fig. 3(d) can be qualitatively explained via the walk-off cancellation of the phase modulation. At any given location of the crystal except the exit layer, the red-shifted front part of the phase-modulated SH pulse can eventually be canceled by the blue-shifted trailing part of the phase modulated SH pulse.[17] Therefore, spectral broadening from 532 to 550 nm or other wavelengths will mainly occur at the end of the crystal where the walk-off between 532 and 1064 nm is insignificant. This is another evidence of XPM. A quantitative analysis is needed to characterize the behavior of the selected band of the spectral broadened SHG XPM signal.

Spectral broadened second-harmonic XPM pulses in ZnSe have been observed to be generated at the exit surface of the nonlinear crystal and are independent to the crystal structure, surface roughness, and temperature. These pulses have been emitted as if they were propagating together with the primary pulse. The observed temporal profile was quantitatively described by the nonphase-matched second-harmonic XPM pulse propagation using the coupled first-order nonlinear differential equations. The temporal and spectral behavior of cross phase modulation may have an important impact in optical communications and information coding.

We thank J. Manassah for theoretical assistance. This research is supported in part by PSC/CUNY and Hamamatus Photonics K. K.

[1] R. R. Alfano, Q. Z. Wang, T. Jimbo, P. P. Ho, R. Bhargava, and B. Fitzpatrick, Phys. Rev. A **35**, 459 (1987).
[2] J. Manassah and O. Cockings, Opt. Lett. **12**, 1005 (1987).
[3] R. Alfano, P. Baldeck, F. Raccah, and P. P. Ho, Appl. Opt. **6**, 3491 (1987).
[4] R. R. Alfano, Q. Li, T. Jimbo, J. Manassah, and P. P. Ho, Opt. Lett. **11**, 626 (1986).
[5] A. R. Chraplyvy, D. Marcuse, and P. S. Henry, Electron. Lett. **20**, 996 (1984).
[6] J. Gersten, R. Alfano, and M. Belic, Phys. Rev. A **21**, 1222 (1980).
[7] M. D. Levenson, R. M. Shelby, M. D. Reid, and D. F. Walls, Phys. Rev. Lett. **57**, 2473 (1987).
[8] R. Fisher, ed., *Optical Phase Conjugation* (Academic, New York, 1983).
[9] P. P. Ho, A. Katz, R. R. Alfano, and N. Schiller, Opt. Commun. **54**, 57 (1985).
[10] H. H. Li, J. Phys. Chem. Ref. Data **13**, 103 (1984).
[11] S. Akhmanov, A. Chirkin, K. Drabovich, and A. Sukhorukov, IEEE J. Quantum Electron. **QE-4**, 598 (1968).
[12] D. Kajzar and J. Messier, in *Nonlinear Optical Properties of Organic Molecules and Crystals*, edited by D. S. Chemla and J. Zyss (Academic, New York, 1987), Vol. 2, p. 81.
[13] N. C. Kothari and X. Carlotti, J. Opt. Soc. Am. B **5**, 756 (1988).
[14] R. W. Hellwarth, *The Order Susceptibilities of Liquids and Solids* (Pergamon, New York, 1977), Prog. Quant. Elect. Vol. 5, pp. 1–68.
[15] D. A. B. Miller, S. D. Smith, and B. S. Wherrett, Opt. Commun. **35**, 221 (1980).
[16] R. Alfano and P. Ho, *Proceedings of Laser '86 Conference* (STS, McLean, VA, 1987), pp. 84–93.
[17] P. Baldeck, R. Alfano, and G. Agrawal, Appl. Phys. Lett. **52**, 1939 (1988).